

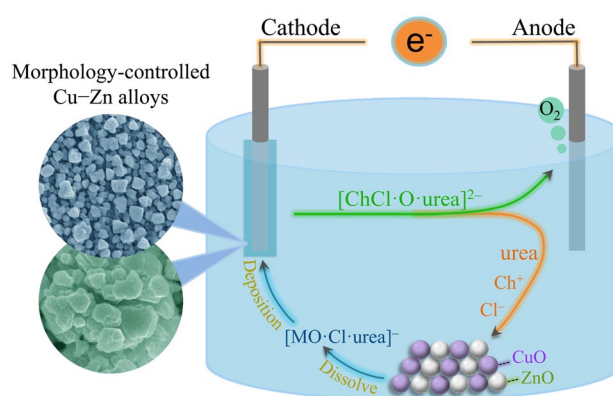
Electrodeposition behavior and characterization of copper–zinc alloy in deep eutectic solvent

Xueliang Xie¹ · Xingli Zou^{1,2} · Xionggang Lu¹ · Qian Xu¹ · Changyuan Lu¹ · Chaoyi Chen³ · Zhongfu Zhou^{1,4}

Received: 25 December 2016 / Accepted: 17 March 2017 / Published online: 25 March 2017
© Springer Science+Business Media Dordrecht 2017

Abstract Cu–Zn alloy films have been electrodeposited directly from their oxide precursors in choline chloride (ChCl)/urea-based deep eutectic solvent (DES). The reaction mechanism and the influence of the cathodic potential on the characteristics of the Cu–Zn alloy films are studied. Cyclic voltammetry and energy dispersive spectroscopy analyses reveal that the reduction of Cu(II) species relatively more preferentially occurs in comparison with the reduction of Zn(II) species, and Cu–Zn codeposition process can be controlled in the DES. Chronoamperometric investigation further confirms that the electrodeposition of Cu–Zn alloy on a Fe electrode follows the three-dimensional instantaneous nucleation-growth process. The micro/nanostructured Cu–Zn alloy films with different phase compositions can be facily produced by controlling the cathodic potential. The obtained Cu–Zn alloy films typically exhibit enhanced corrosion resistances in 3 wt% NaCl aqueous solution. It is suggested that Cu–Zn alloy films can be sustainably electrodeposited from their abundant and inexpensive oxide precursors in DES.

Graphical Abstract Micro/nanostructured Cu–Zn alloy films have been electrodeposited directly from CuO and ZnO precursors in deep eutectic solvent (DES), the electrochemical reaction mechanism and the nucleation-growth process of Cu–Zn alloy in the DES are investigated.



Keywords Electrodeposition · Deep eutectic solvent · Cu–Zn alloy · Oxides · Nucleation-growth kinetics

✉ Xingli Zou
xzou@utexas.edu

✉ Xionggang Lu
luxg@shu.edu.cn

¹ State Key Laboratory of Advanced Special Steel & Shanghai Key Laboratory of Advanced Ferrometallurgy & School of Materials Science and Engineering, Shanghai University, Shanghai 200072, People's Republic of China

² Center for Electrochemistry, Department of Chemistry, The University of Texas at Austin, Austin, TX 78712, USA

³ School of Materials and Metallurgy, Guizhou University, Guiyang 550025, China

⁴ Institute of Mathematics and Physics, Aberystwyth University, Aberystwyth SY23 3BZ, UK

1 Introduction

Cu–Zn alloy plays an important role in a large range of industrial applications such as corrosion resistance, electrocatalysis, electronics, etc [1–3]. Traditionally, electrodeposition of Cu–Zn alloy is performed in aqueous electrolyte solutions with high conductivity and low fabrication cost. However, the electrodeposition carried out in the cyanide- and acid-based aqueous solutions generally involves high corrosiveness and hydrogen-evolution process [4]. Therefore, exploring for ideal electrolyte

candidates for the Cu–Zn alloy electrodeposition at or near room temperature is required. Considerable attention has been focused on the use of ionic liquids as electrolyte media for the electrodeposition of metals/alloys in recent years [5, 6]. Compared with aqueous solutions, ionic liquids (ILs) usually have wide electrochemical windows, extremely low vapor pressure, high ionic conductivity, high solubility of metal salts, and thermal stability [6, 7]. The electrodeposition of Cu–Zn alloy in ionic liquid electrolytes has been preliminarily proven. Sun et al. [2, 8] investigated the electrodeposition of Cu–Zn alloy in Lewis acidic $\text{ZnCl}_2/1\text{-ethyl-3-methylimidazolium chloride}$ ionic liquids. It was found that the surface morphologies of the electrodeposits can be influenced by the electrodeposition potential, temperature, and metal concentration of the electrolyte. In addition, Rousse et al. [9] studied the electrodeposition of Cu, Zn, and Cu–Zn alloy in the 1-butyl-1-methylpyrrolidinium bis(trifluoromethylsulfonyl)imide ionic liquid. In these cases, the use of ionic liquids can avoid the problem associated with hydrogen embrittlement, and nanocrystalline Cu–Zn electrodeposits can be readily obtained without any additive during the alloy electrodeposition. However, the corrosiveness, cost, and the instability against air and moisture of these ionic liquids probably restrict their further practical application [9, 10]. In addition, many copper/zinc salts such as halides generally have very low solubilities in the ionic liquids [11]. The copper/zinc cations can be introduced into the Tf_2N -based ionic liquids by anodic dissolution of copper/zinc electrodes [11, 12] or by dissolution of copper/zinc- Tf_2N salts [9]; however, these processes are time consuming. Consequently, suitable copper/zinc precursor–electrolyte systems are extremely needed for the electrodeposition of Cu–Zn alloy at low temperature.

Deep eutectic solvents (DESs), which are formed by mixing quaternary ammonium salts with hydrogen bond donor species such as alcohols, amides, and carboxylic acids [13, 14], have been considered as alternative media due to their biodegradation, nontoxicity, facile synthesis at low cost, and stability in air and water [13–15]. The DESs have been extensively used in a range of fields including material synthesis [16], dissolution and extraction processes [17, 18], and electrodeposition [19, 20]. Furthermore, they are capable of dissolving a wide range of metal oxides with high selectivities [21, 22]. Compared with metal chloride precursors (e.g., CuCl_2 , ZnCl_2 , etc.) [7], the abundant and inexpensive metal oxides (e.g., CuO, ZnO, etc.) can be used as new precursors for the green and facile electrodeposition of alloy films in DESs without chloridization pretreatment. The remarkable dissolving capacity contributes to the processing of metal oxides and probably provides a green electrochemistry pathway for the production of metals/alloys directly from their oxide precursors

in DESs at room temperature. Abbott et al. [23] pioneered their study on the large-scale extraction and separation of metals from a complex matrix using DESs. Hussey et al. [24] investigated the electrochemistry of Cu_2O and the nucleation/growth mechanism of Cu electrodeposition in ChCl/urea -based DES. Reddy et al. [25, 26] studied the electrodeposition of zinc and lead films from their oxides in the same DES due to its appreciable solvent power. In addition, Zhang et al. [27–29] reported that the DESs can be used as alternative solvents to prepare metals from solid oxides by in situ electroreduction. In our recent study [30, 31], micro/nanostructured Zn and Cu films have also been electrodeposited from ZnO and CuO precursors in DESs, respectively. Therefore, it is reasonable to believe that the electrodeposition of Cu–Zn alloy from their oxide precursors in DESs is possible. However, the electrodeposition process for Cu–Zn alloy in ChCl/urea -based DES has not been systematically investigated. Particularly, the reaction mechanism of the electrodeposition process and the nucleation-growth process of Cu–Zn alloy in the DES are not well understood and need further investigation.

In the current study, we report the electrodeposition of Cu–Zn alloy from CuO and ZnO precursors in ChCl/urea -based DES. The electrochemical reaction mechanism and the nucleation-growth process of Cu–Zn alloy on a Fe substrate in the DES are presented. The influences of the cathodic electrodeposition potential on the phase composition, structure, morphology, and corrosion behavior of the electrodeposited Cu–Zn alloy are determined.

2 Experimental

Choline chloride [$\text{HOC}_2\text{H}_4\text{N}(\text{CH}_3)_3\text{Cl}$] (ChCl) (Aldrich 98%), urea [NH_2CONH_2] (Aldrich 99.5%), CuO (Aldrich 99.5%), and ZnO (Aldrich 99.5%) were dried under vacuum prior to use. The eutectic solvent was obtained by stirring the mixture of ChCl and urea in a molar ratio of 1:2 (12CU) at 343 K until the formation of a homogeneous, colorless solution. Then, the electrolyte was prepared by dissolving 0.01 M CuO and 0.1 M ZnO in the 12CU ionic liquid at 343 K. The concentrations of the dissolved copper and zinc species (mainly in forms $[\text{CuO}\cdot\text{Cl}\cdot\text{urea}]^-$ and $[\text{ZnO}\cdot\text{Cl}\cdot\text{urea}]^-$) [24–31] in the CuO/ZnO-saturated 12CU ionic liquid at 343 K were determined to be about 0.016 and 0.342 M, respectively.

Electrochemical investigations including cyclic voltammetry (CV), chronoamperometry (CA), and potentiodynamic polarization were carried out under an argon atmosphere by means of a HCP-803 electrochemical workstation (BioLogic). About 60 mL of the prepared 12CU ionic liquid containing 0.01 M CuO and 0.1 M ZnO served as the electrolyte for these experiments. A three-electrode

system, comprising a platinum plate ($S=0.6\text{ cm}^2$) as the counter electrode, a Fe electrode ($S=0.5\text{ cm}^2$) as the working electrode, and a silver wire (1.0 mm in diameter) as the reference electrode, was used during the electrochemical experiments. All the electrodes were polished with $0.3\text{ }\mu\text{m}$ alumina paste, rinsed, and dried prior to all measurements. It is worth noting that the silver wire acted as the quasi-reference electrode in the electrochemical experiments [32]. All electrochemical experiments (CV and CAs) were performed at 343 K. Following the electrodeposition experiments, the samples were taken out, washed with distilled water and alcohol, and then dried rapidly.

The corrosion behavior of the Cu–Zn electrodeposits was investigated by polarization experiment in 3 wt% NaCl aqueous solution. A three-electrode system consisting of a platinum plate counter electrode, an Ag/AgCl (saturated with KCl) reference electrode, and the sample working electrode (surface area of about 0.5 cm^2) was used. The samples remained at the open-circuit potential (OCP) for 30 min before polarization experiments. The OCP values of the samples obtained at different electrodeposition potentials are stable in the potentials ranging from -0.39 to -0.79 V . Polarization curves were recorded at a scan rate of 5 mV s^{-1} from -200 to $+200\text{ mV}$ vs. E_{OCP} . Based on the Tafel extrapolation method, the corrosion potential (E_{corr}) and corrosion current density (j_{corr}) were determined.

The macro- and microstructures of the electrodeposited Cu–Zn alloy films were characterized by means of an optical microscope (KEYENCE VHX-1000C) and a scanning electron microscope (SEM, JEOL JSM-6700F), respectively. The elemental composition of the samples was analyzed by energy dispersive spectroscopy (EDS, Oxford INCA EDS system). The phase structure of the samples was examined by X-ray diffraction (XRD, Bruker-AXS D8 Advance) with Cu $K\alpha$ radiation at a scan rate of 5° min^{-1} , and the target voltage and tube current were 40 kV and 40 mA, respectively. The concentrations of the dissolved copper and zinc species in the CuO/ZnO-saturated 12CU ionic liquid were determined by inductively coupled plasma spectroscopy (ICP, Perkin Elmer PE400).

3 Results and discussion

3.1 CV analysis

Figure 1a shows the CV curve of a Fe electrode in pure 12CU ionic liquid at 343 K with a scan rate of 10 mV s^{-1} . In the pure 12CU system, the cathodic potential limit is about -1.20 V . Fig. 1b shows the CV curve of the 12CU ionic liquid containing 0.01 M CuO and 0.1 M ZnO on a Fe electrode at 343 K with a scan rate of 10 mV s^{-1} . Three reduction peaks are observed in the cathodic

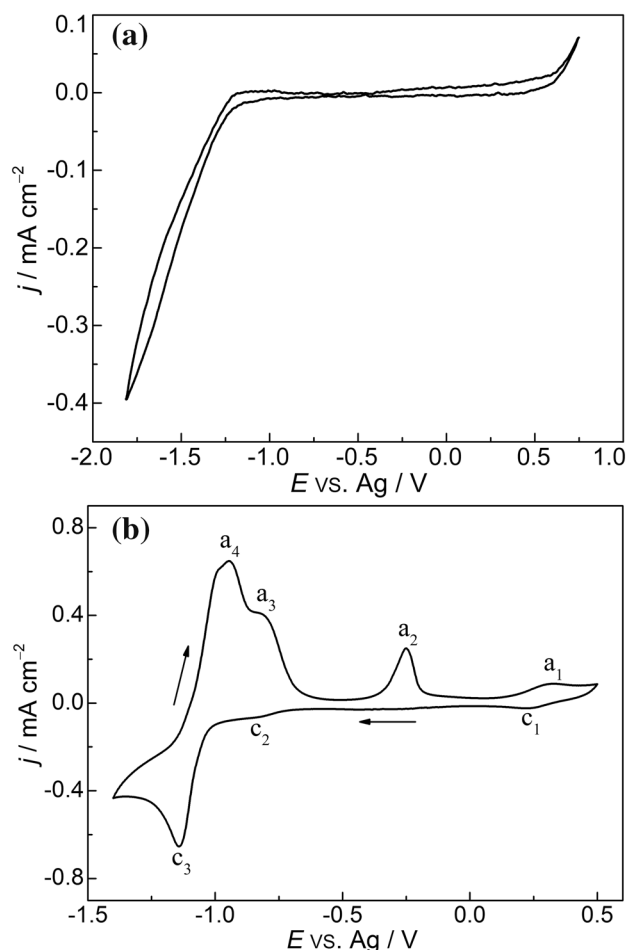


Fig. 1 **a** Cyclic voltammogram for a Fe electrode in pure 12CU ionic liquid at 343 K with a scan rate of 10 mV s^{-1} . **b** Cyclic voltammogram for a Fe electrode immersed in 12CU ionic liquid containing 0.01 M CuO and 0.1 M ZnO at 343 K with a scan rate of 10 mV s^{-1}

range. The reduction peaks (c_1 , c_2) and their corresponding oxidation peaks (a_1 , a_2) are attributed to the reduction and oxidation processes of Cu(II)/Cu(I) and Cu(I)/Cu(0), respectively [31]. The reduction peak c_3 is associated with the cathodic formation of Cu–Zn electrodeposits, which can be confirmed by the EDS analysis (Fig. 2). The EDS spectra reveal that the electrodeposits produced at -0.80 V (reduction peak c_2 illustrated in Fig. 1b) and 343 K for 2 h on a Fe substrate contain 100 wt% Cu (Fig. 2a), while the electrodeposits produced at -1.15 V (reduction peak c_3 illustrated in Fig. 1b) and 343 K for 2 h on a Fe substrate contain 20.1 wt% Cu and 79.9 wt% Zn (Fig. 2b). Results from CV and EDS analyses indicate that Cu–Zn codeposition occurs at a potential more negative than that of the electrodeposition of pure Cu, and the electrodeposition of Cu–Zn in 12CU ionic liquid is not the anomalous codeposition [33, 34]. On the reverse scan, the apparent oxidation peaks a_3 and a_4 are mainly

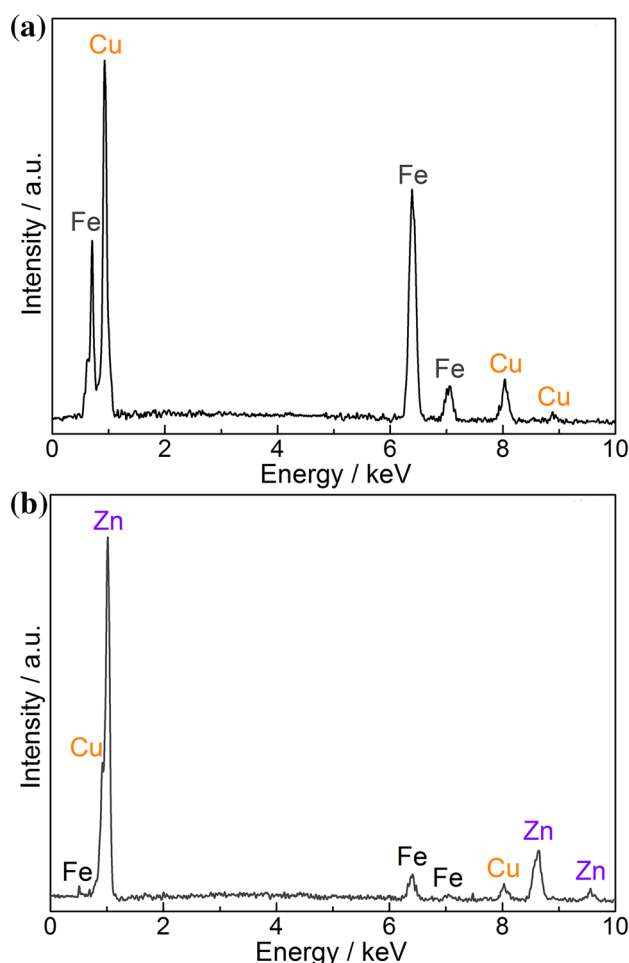


Fig. 2 EDS analysis of the Cu–Zn electrodeposits obtained on a Fe substrate in 12CU ionic liquid containing 0.01 M CuO and 0.1 M ZnO at **a** -0.80 V, **b** -1.15 V and 343 K for 2 h

related to the stripping of Cu–Zn electrodeposits and pure Zn, respectively [30, 33].

3.2 Chronoamperometric investigations

To study the nucleation-growth mechanism of Cu–Zn electrodeposition, chronoamperometric experiments were carried out in 12CU ionic liquid containing 0.01 M CuO and 0.1 M ZnO at 343 K, and the current density–time transients resulting from these tests are illustrated in Fig. 3. The current transients show the typical profile for a three-dimensional multiple nucleation with diffusion-limited growth [34]. The sharp decrease of current density in each transient is due to the charging of the double layer, and the attendant increase in current density is attributed to the formation and growth of Cu/Zn nuclei [35]. Then the current density decreases after reaching a maximum current density j_m at the time of t_m . Furthermore, the j_m increases, and the t_m decreases with the increasing nucleation potential,

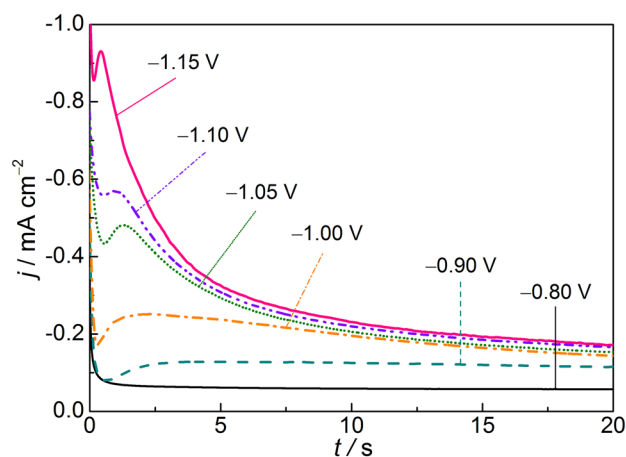


Fig. 3 Current density–time transients resulting from chronoamperometric experiments on a Fe electrode in 12CU ionic liquid containing 0.01 M CuO and 0.1 M ZnO at 343 K

which is mainly ascribed to the decrease in time needed for overlapping of the diffusion zones [34].

A conventional approach to analyze the nucleation-growth mechanism was put forward by Scharifker and Hills [36]. The most famous models for describing the kinetics of the initial stages of the electrocrystallization process are instantaneous and progressive nucleation models. The instantaneous nucleation model means that all the nuclei are formed within very short times after the potential step, while progressive nucleation model means that the nucleation will gradually take place and precious nucleation sites continue to grow. To distinguish between the two cases of nucleation, the experimental current density–time transients are compared with the theoretical transients, and the expressions of instantaneous (Eq. 1) and progressive (Eq. 2) nucleations are represented, respectively.

$$(j_{\text{inst}}/j_m)^2 = 1.9542(t/t_m)^{-1} \{1 - \exp[-1.2564(t/t_m)]\}^2 \quad (1)$$

$$(j_{\text{prog}}/j_m)^2 = 1.2254(t/t_m)^{-1} \{1 - \exp[-2.3367(t/t_m)^2]\}^2 \quad (2)$$

Figure 4 shows the comparison of the experimental transients with the theoretical models for instantaneous and progressive nucleations during the Cu–Zn alloy electrodeposition in 12CU ionic liquid. The electrodeposition of Cu–Zn alloy on a Fe electrode follows the three-dimensional instantaneous nucleation-growth process. Similarly, the three-dimensional instantaneous nucleation-growth process was also observed in the previous studies for the electrodeposition of Zn on a Cu electrode in 12CU ionic liquid [25, 30]. It is indicated that the electronegative metal Zn involves instantaneous nucleation-growth mechanism irrespective of substrate material in 12CU ionic liquid [37].

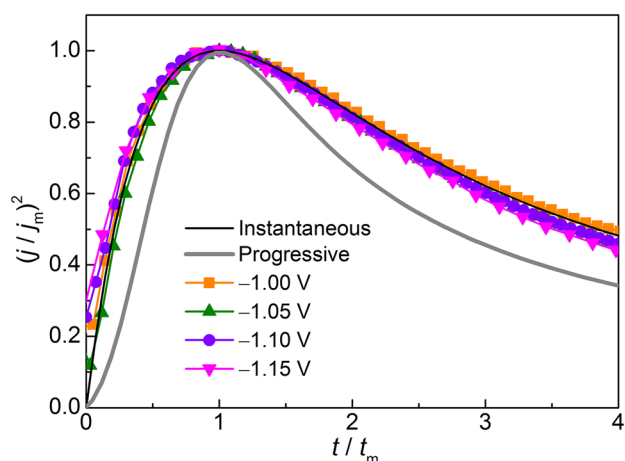


Fig. 4 Comparison of the dimensionless experimental data derived from Fig. 3 with the theoretical models for three-dimensional nucleation process

Moreover, due to the presence of Cu(II) ion, the Cu(II) and Zn(II) ions would compete for the nucleation site, the formation of Cu–Zn alloy phase structure is dependent on the nucleation mechanism, *i.e.*, the nucleation rate and the competition between nucleation and growth [38]. The instantaneous nucleation tends to form an alloy phase which is a solid solution, while progressive nucleation tends to form a phase which has a small amount of one species inserted in the matrix of the other major species [38]. Therefore, the electrodeposition of Cu–Zn on a Fe electrode in 12CU ionic liquid is likely to form a solid solution, which can be further confirmed by the XRD analysis (Fig. 8).

3.3 Electroreduction process of Cu(II)/Zn(II) species in 12CU ionic liquid

The Cu–Zn alloy electrodeposition was carried out on a Fe substrate in 12CU ionic liquid containing 0.01 M CuO and 0.1 M ZnO at different electrodeposition potentials and 343 K for 2 h. Based on the previous study [23–25, 28–31], the 12CU ionic liquid dissolved with CuO and ZnO can form complex species $[\text{CuO} \cdot \text{Cl} \cdot \text{urea}]^-$ and $[\text{ZnO} \cdot \text{Cl} \cdot \text{urea}]^-$ (Reaction 3). The structure of $\text{HOC}_2\text{H}_4\text{N}(\text{CH}_3)_3^+$ (expressed as Ch^+) is not destroyed in the 12CU–CuO (0.01 M) and 12CU–ZnO (0.1 M) systems [24, 31]. Therefore, the $[\text{CuO} \cdot \text{Cl} \cdot \text{urea}]^-$, $[\text{ZnO} \cdot \text{Cl} \cdot \text{urea}]^-$ and Ch^+ ions can diffuse through the electrolyte and react at cathode to form Cu–Zn alloy and $[\text{ChCl} \cdot \text{O} \cdot \text{urea}]^{2-}$ (Reaction 4). The complex anion $[\text{ChCl} \cdot \text{O} \cdot \text{urea}]^{2-}$ is formed among ChCl , urea and O^{2-} anion, which can be confirmed by the previous study [25, 28, 29]. Then, the formed $[\text{ChCl} \cdot \text{O} \cdot \text{urea}]^{2-}$ complex anion can traverse through the electrolyte and lose electrons at anode to generate gas (Reaction 5) [25, 28, 29]. The anode gas generally consists of O_2 , whereas a small amount of Cl_2 may

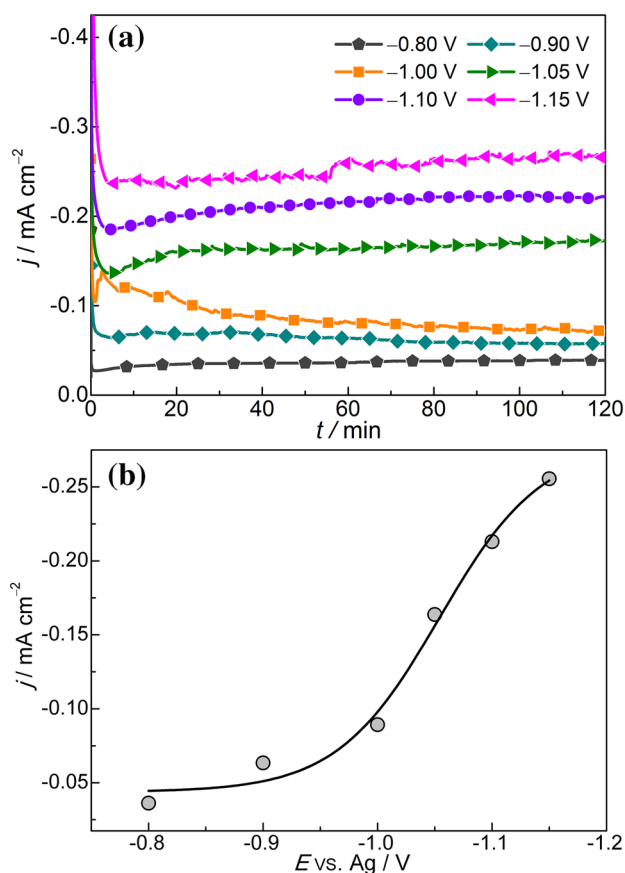
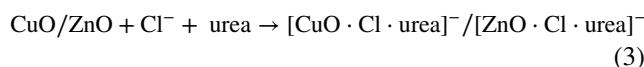


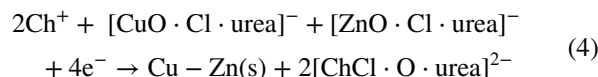
Fig. 5 a Variation of current density with time for different electrodeposition potentials in 12CU ionic liquid containing 0.01 M CuO and 0.1 M ZnO at 343 K for 2 h. b Variation of average current density with electrodeposition potential at 343 K for 2 h

appear when the cathodic electrodeposition potential is higher than the decomposition potential of the electrolyte [39, 40]. Hence, the possible reactions are as follows.

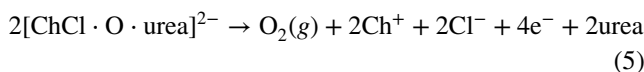
Dissolution reaction



Cathodic reaction



Anodic reaction



3.4 Electrodeposition and characterization of Cu–Zn alloy

The effect of the cathodic electrodeposition potential on the current density and the characteristics of the Cu–Zn alloy

films in 12CU ionic liquid were studied in the potentials ranging from -0.80 to -1.15 V at 343 K. Variation of current density with time is shown in Fig. 5a. The current density increases with more negative potential. However, the current densities almost maintain at relatively stable values with the increasing electrodeposition time, even at more negative potentials. It is indicated that the electrodeposition of Cu–Zn alloy in 12CU ionic liquid is a stable and fast electrochemical process. Figure 5b shows the variation of the average current density with electrodeposition potential. It is obvious that the average current density increases with the increasing electrodeposition potential. More negative potential can accelerate the reduction reaction, and thus contribute to higher current density during the electrodeposition process.

The elemental compositions (determined by EDS) of the electrodeposited Cu–Zn alloy films are found to be a function of the cathodic potential, as shown in Fig. 6. All electrodeposits are only composed of Cu and Zn

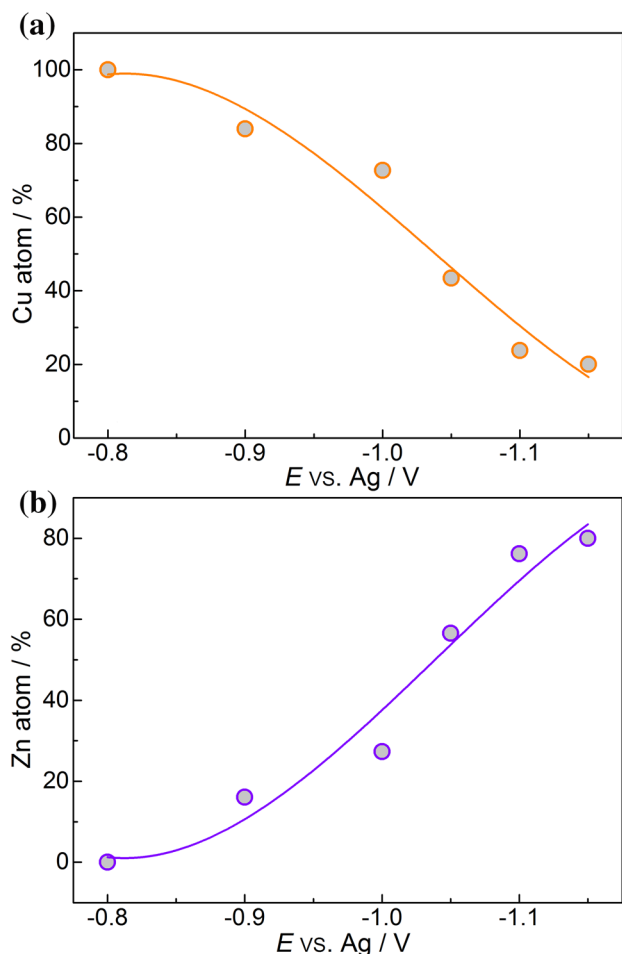


Fig. 6 **a** Cu and **b** Zn contents of the Cu–Zn alloys electrodeposited in 12CU ionic liquid containing 0.01 M CuO and 0.1 M ZnO at different electrodeposition potentials and 343 K for 2 h

without impurity. In the Cu–Zn electrodeposits, Cu content decreases and Zn content increases with the increasing cathodic potential. The different Cu and Zn compositions can be attributed to their different electrodeposition rates and different solubilities (ZnO: 0.342 M; CuO: 0.016 M) in 12CU ionic liquid at 343 K.

Figure 7 shows the optical microscopic images of the surfaces of the Cu–Zn alloy films electrodeposited at different cathodic potentials and 343 K for 2 h. Homogenous Cu and Cu–Zn alloy films can be electrodeposited from CuO and ZnO precursors in the potential range of -0.80 to -1.15 V (Fig. 7a–f). However, the Cu–Zn alloy films electrodeposited at -0.90 to -1.15 V exhibit different appearances (Fig. 7b–f). The different appearances are mainly due to the different compositions of the Cu–Zn electrodeposits (corresponding to Fig. 6).

XRD patterns of the Cu–Zn alloy films electrodeposited on a Fe substrate at different cathodic potentials and 343 K for 2 h are shown in Fig. 8. The pure Cu electrodeposit produced at -0.80 V shows two diffraction peaks at 2θ (43.3° and 50.4°), which correspond to the characteristic of (1 1 1) and (2 0 0), respectively. At more negative potentials of -0.90 and -1.00 V, the diffraction peaks of the electrodeposits become broader and smoother, and shift to slightly lower 2θ values compared to those of pure Cu. These changes can be attributed to the formation of α -CuZn phases in the electrodeposits or zinc solid solution in copper [41], which is consistent with the instantaneous nucleation-growth process. More negative potential can contribute to a higher electrodeposition rate, and hence form the nanocrystalline electrodeposits. The average crystal sizes of the Cu and α -CuZn phases obtained at -0.80 , -0.90 , and -1.00 V were calculated by XRD (Fig. 8) using Scherrer equation [42] with the TOPAS software, and the values are approximately 18.3, 9.9, and 5.5 nm, respectively. However, the diffraction peaks of the Cu–Zn film electrodeposited at -1.05 V are different from those of the samples electrodeposited at -0.80 , -0.90 , and -1.00 V. For the Cu–Zn film electrodeposited at -1.05 V, the dominant phase is Cu_5Zn_8 , which further confirms that the codeposition of Cu–Zn alloy can be achieved by controlling the cathodic potential. The average crystal size of the Cu_5Zn_8 phase is about 39.9 nm. For more negative potentials (-1.10 and -1.15 V), the Cu_5Zn_8 phase rapidly disappears, and the ϵ - CuZn_5 , Zn phases are clearly visible, owing to the increased Zn electrodeposition rate at more negative potential [41]. The observation is consistent with the EDS analysis mentioned above (Fig. 6). The calculated average crystal sizes for the CuZn_5 and Zn phases obtained at -1.10 and -1.15 V are 48.5, 20.4, and 39.4, 72.0 nm, respectively. The results of the formation of various Cu–Zn alloy films at different cathodic potentials are similar to the

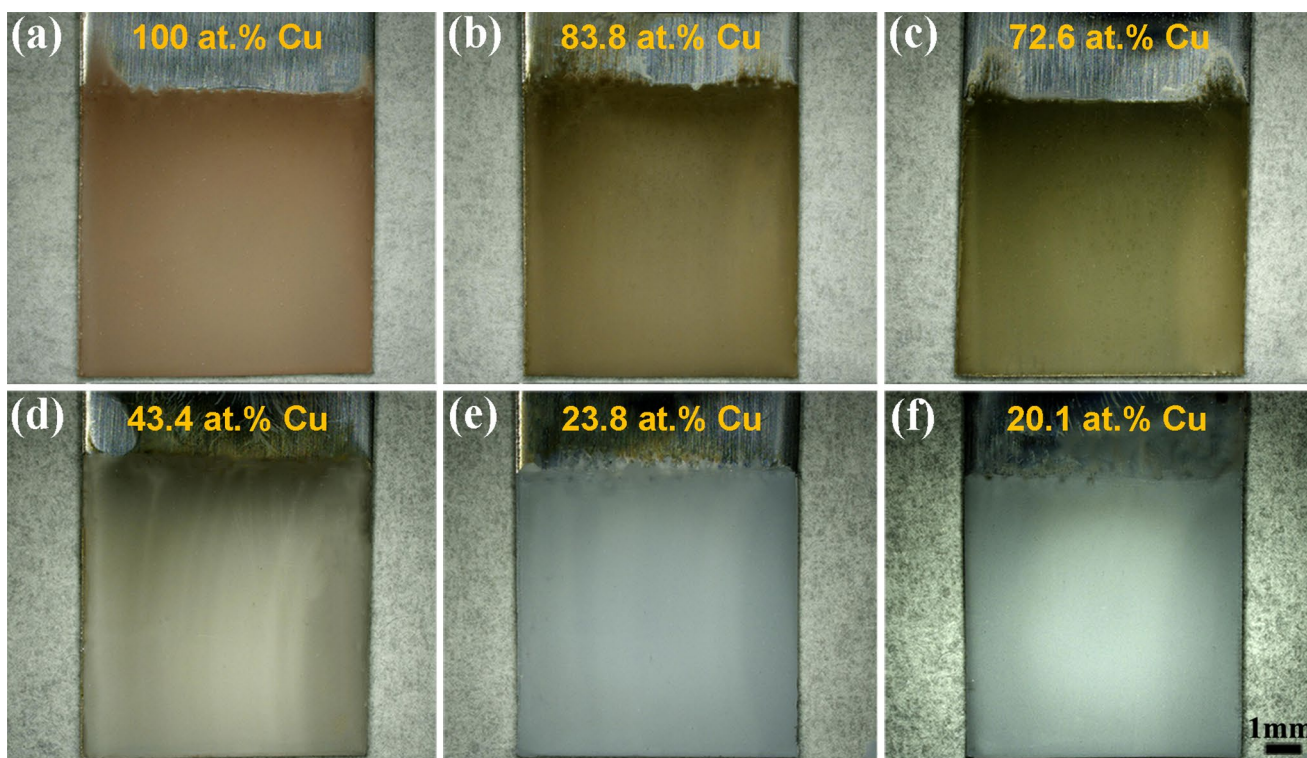


Fig. 7 Optical microscopic images of the surfaces of the Cu–Zn alloy films electrodeposited in 12CU ionic liquid containing 0.01 M CuO and 0.1 M ZnO at the potentials of **a** –0.80 V, **b** –0.90 V, **c** –1.00 V, **d** –1.05 V, **e** –1.10 V, **f** –1.15 V, and 343 K for 2 h

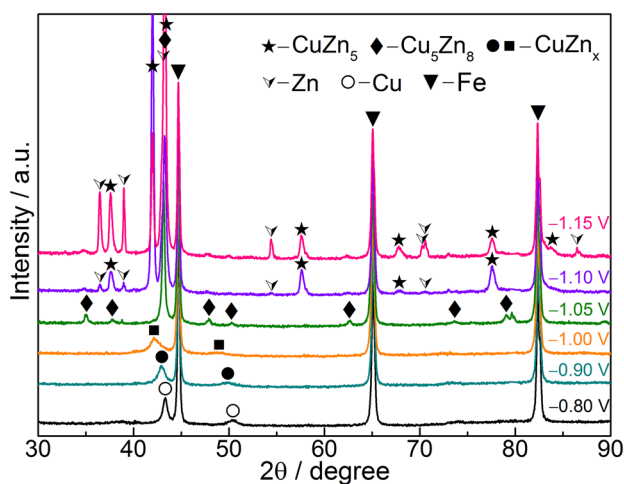


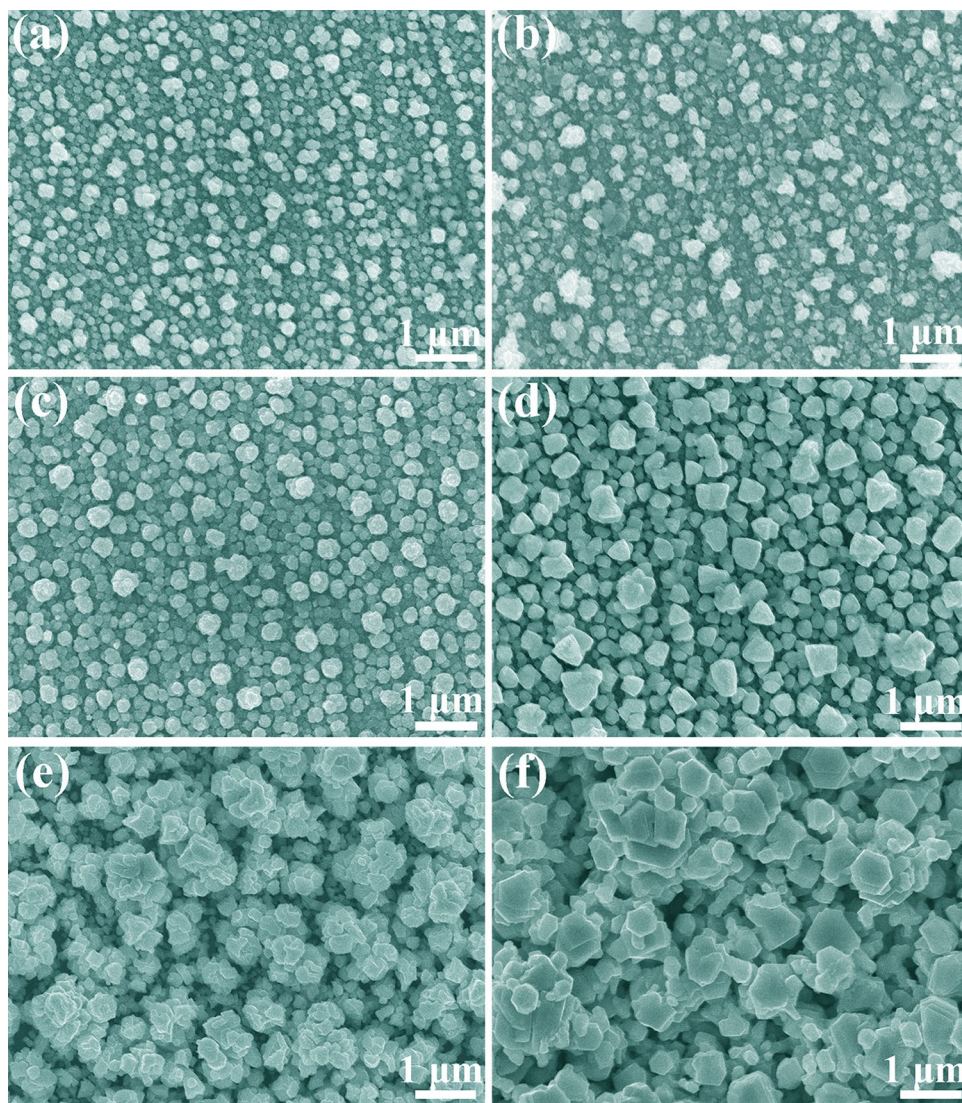
Fig. 8 XRD patterns of the electrodeposited Cu–Zn alloy films obtained on a Fe substrate in 12CU ionic liquid containing 0.01 M CuO and 0.1 M ZnO at different electrodeposition potentials and 343 K for 2 h

results reported for the electrodeposition of Cu–Zn alloy films in the pyrophosphate solution [43].

The surface morphologies of the Cu–Zn alloy films electrodeposited on a Fe substrate at different cathodic potentials and 343 K for 2 h are illustrated in Fig. 9.

The pure Cu film electrodeposited at –0.80 V consist of spherical nodules (Fig. 9a), and showing an optically fuchsia color in appearance (Fig. 7a). When the electrodeposition potential is changed to –0.90 V (Fig. 9b) where Cu–Zn codeposition occurs, a relatively looser and rougher surface is produced, and the electrodeposits exhibit a brown color in appearance (Fig. 7b). As the electrodeposition potential increases to –1.00 V (Fig. 9c), the Cu–Zn electrodeposits are made up of spherical clusters. Upon further increasing the electrodeposition potential to –1.05 V (Fig. 9d), the polygonal structures of particles are observed, and the Cu–Zn electrodeposits exhibit a gray color in appearance (Fig. 7d), due to the Zn electrodeposition rate increases with more negative potential. For more negative potentials of –1.10 and –1.15 V (Fig. 9e, f), the hexagonal ϵ -CuZn₅ phase begins to form at the higher quantity of Zn in the alloy [41]. Combining with the average crystal sizes of CuZn₅ and Zn phases calculated from Fig. 8 (CuZn₅: 48.5 nm, Zn: 20.4 nm at –1.10 V; CuZn₅: 39.4 nm, Zn: 72.0 nm at –1.15 V), the formations of the hexagonal-shaped Zn and Cu–Zn alloy particles are mainly ascribed to the agglomeration of Cu and Zn crystals [30, 44]. More negative potential can contribute to the aggregation of the particles, resulting in the formation of the large particles [31, 45]. In addition, the content of Zn obviously increases

Fig. 9 SEM images of the Cu–Zn alloy electrodeposited on a Fe substrate in 12CU ionic liquid containing 0.01 M CuO and 0.1 M ZnO at the potentials of **a** -0.80 V, **b** -0.90 V, **c** -1.00 V, **d** -1.05 V, **e** -1.10 V, **f** -1.15 V and 343 K for 2 h



with the increasing electrodeposition potential, and the Cu–Zn electrodeposits become less uniform and less compact, showing silver-colored appearances (Fig. 7e, f). Based on the EDS, XRD, and SEM analyses, it is evident that the phase composition, structure, and morphology of the Cu–Zn alloy films electrodeposited in 12CU ionic liquid containing 0.01 M CuO and 0.1 M ZnO can be readily tuned by controlling the cathodic electrodeposition potential. Furthermore, it is worth noting that the concentration ratios of the precursors in the electrodeposition bath have significant influences on the resultant composition, microstructure, and property of the alloy electrodeposits. Different Cu/Zn concentration ratios would contribute to different electrodeposition rates and thus influence the Cu–Zn alloy electrodeposition process [46, 47].

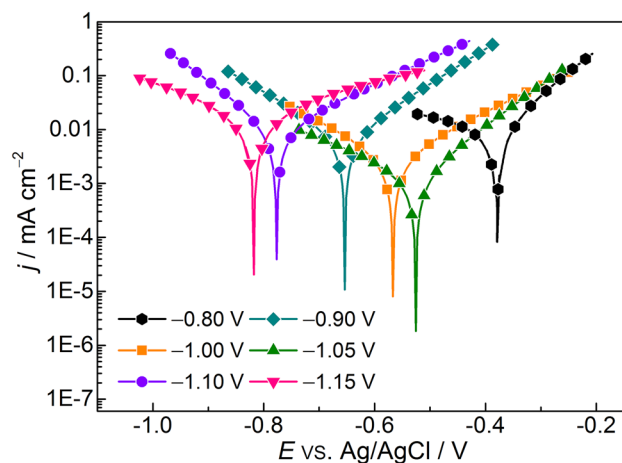


Fig. 10 Polarization curves of the electrodeposited Cu–Zn alloy films obtained at different electrodeposition potentials in 3 wt% NaCl aqueous solution at room temperature

3.5 Corrosion performance of the Cu–Zn alloy films

The polarization curves obtained from potentiodynamic polarization tests for Cu–Zn alloy films electrodeposited at different cathodic potentials in 3 wt% NaCl solution at room temperature are shown in Fig. 10. The corrosion potentials (E_{corr}) and corrosion current densities (j_{corr}) obtained from the polarization curves (Fig. 10) for Cu–Zn alloy films are summarized in Table 1. It is obvious that the E_{corr} of the sample generally decreases with the increasing electrodeposition potential, and this can be attributed to the increased Zn content of the electrodeposits [30]. The microstructure and phase composition of the Cu–Zn alloy films would influence their corrosion resistances [48]. The Cu–Zn alloy film electrodeposited at -1.15 V and 343 K displays the lowest E_{corr} of about -817 mV and the highest j_{corr} of about $12.23 \mu\text{A cm}^{-2}$, which is even worse than pure Cu film electrodeposited at -0.80 V and 343 K (the Zn content is 0%). The poor corrosion resistance of the Cu–Zn alloy film electrodeposited at -1.15 V and 343 K may be ascribed to its coarse, non-uniform structure and its higher Zn content. However, the Cu–Zn alloy film electrodeposited at -1.05 V and 343 K shows enhanced corrosion resistance. The E_{corr} of the specimen is increased to about -526 mV, and the j_{corr} is decreased to approximately $1.86 \mu\text{A cm}^{-2}$. Compared with the previous Zn film electrodeposited in the same DES ($E_{\text{corr}} = -806$ mV, $j_{\text{corr}} = 12.05 \mu\text{A cm}^{-2}$) [30], the Cu–Zn alloy films electrodeposited at the moderate potentials (from -0.90 to -1.05 V) show enhanced corrosion resistance (Table 1). The enhanced corrosion resistance is likely to be mainly attributed to the compact and uniform microstructure of the Cu–Zn alloy film [48, 49]. And also, the Cu–Zn alloy films containing 27.4–56.6 at.% Zn exhibit improved corrosion resistances compared to that of the commercial Cu–40Zn alloy and the Ni–Zn electrodeposit with Zn content of 88.72 at.% being obtained in aqueous solution [50, 51], which can be verified by the lower j_{corr} in Table 1.

Table 1 Corrosion characteristics of the electrodeposited Cu–Zn alloy films summarized from potentiodynamic polarization tests in 3 wt% NaCl aqueous solution at room temperature

Conditions	Zn content(at.%)	E_{corr} (mV)	j_{corr} ($\mu\text{A cm}^{-2}$)
-0.80 V	0	-378	10.45
-0.90 V	16.2	-656	5.63
-1.00 V	27.4	-567	2.54
-1.05 V	56.6	-526	1.86
-1.10 V	76.2	-776	9.52
-1.15 V	79.9	-817	12.23
Cu–40Zn alloy [50]	38.19	-232	32
Ni–Zn electrodeposit [51]	88.72	-1014	40.20

4 Conclusions

The electrodeposition behavior of Cu–Zn alloy in 12CU ionic liquid containing 0.01 M CuO and 0.1 M ZnO was investigated. The reaction mechanism involved in the electrodeposition process and the influence of the cathodic potential on the characteristics of the Cu–Zn alloy films were discussed. Voltammetric measurement shows that the reduction potential of Cu(II) species is more positive than that of Zn(II) species, and Cu–Zn codeposition can be achieved at a potential more negative than that of Cu electrodeposition. Three-dimensional instantaneous nucleation-growth process is occurred on the electrodeposition of Cu–Zn alloys. By controlling the electrodeposition potential, uniform and compact Cu–Zn electrodeposits can be produced. The phase composition and structure of the Cu–Zn alloys are significantly dependent on the electrodeposition potential. Moreover, the Cu–Zn alloy films electrodeposited at the moderate electrodeposition potentials (from -0.90 to -1.05 V) typically exhibit enhanced corrosion resistances in 3 wt% NaCl aqueous solution. The study reveals that the abundant and inexpensive CuO and ZnO can be used as novel candidate precursors for the electrodeposition of Cu–Zn alloy films in 12CU ionic liquid at room temperature, and the electrochemical process can be facilely and effectively controlled.

Acknowledgements The authors thank China National Funds for Distinguished Young Scientists (No. 51225401), the National Natural Science Foundation of China (Nos. 51574164, 51304132 and 51664005), the National Basic Research Program of China (No. 2014CB643403), the Science and Technology Commissions of Shanghai Municipality (No. 14JC1491400) and the Young Teacher Training Program of Shanghai Municipal Education Commission for financial support. We also thank the Instrumental Analysis and Research Center of Shanghai University for materials characterization.

References

- Milošev I, Mikić TK, Gaberšček M (2006) The effect of Cu-rich sub-layer on the increased corrosion resistance of Cu–xZn alloys in chloride containing borate buffer. *Electrochim Acta* 52:415–426. doi:10.1016/j.electacta.2006.05.024
- Hsieh YT, Tsai RW, Su CJ, Sun IW (2014) Electrodeposition of CuZn from chlorozincate ionic liquid: from hollow tubes to segmented nanowires. *J Phys Chem C* 118:22347–22355. doi:10.1021/jp506833s
- Zhang P, An XH, Zhang ZJ, Wu SD, Li SX, Zhang ZF, Figueiredo RB, Gao N, Langdon TG (2012) Optimizing strength and ductility of Cu–Zn alloys through severe plastic deformation. *Scr Mater* 67:871–874. doi:10.1016/j.scriptamat.2012.07.040
- Paatsch W (2010) Hydrogen embrittlement in electroplating: avoidance using pulse plating. *Trans Inst Met Finish* 88:277–278. doi:10.1179/002029610X12791981507848
- Mais L, Mascia M, Vacca A, Palmas S, Delogu F (2015) Electrochemical deposition of Cu and Ta from pyrrolidinium based

- ionic liquid. *J Appl Electrochem* 45:735–744. doi:[10.1007/s10800-015-0824-1](https://doi.org/10.1007/s10800-015-0824-1)
6. Endres F, Abbott AP, MacFarlane DR (2008) *Electrodeposition from ionic liquids*. Wiley-VCH, Weinheim
 7. Hartley JM, Ip CM, Forrest G, Singh K, Gurman SJ, Ryder KS, Abbott AP, Frisch G (2014) EXAFS study into the speciation of metal salts dissolved in ionic liquids and deep eutectic solvents. *Inorg Chem* 53:6280–6288. doi:[10.1021/ic500824r](https://doi.org/10.1021/ic500824r)
 8. Chen PY, Lin MC, Sun IW (2000) Electrodeposition of Cu–Zn alloy from a Lewis acidic ZnCl₂–EMIC molten salt. *J Electrochem Soc* 147:3350–3355. doi:[10.1149/1.1393905](https://doi.org/10.1149/1.1393905)
 9. Rousse C, Beaufile S, Fricoteaux P (2013) Electrodeposition of Cu–Zn thin films from room temperature ionic liquid. *Electrochim Acta* 107:624–631. doi:[10.1016/j.electacta.2013.06.053](https://doi.org/10.1016/j.electacta.2013.06.053)
 10. Endres F, Zein El Abedin S (2006) Air and water stable ionic liquids in physical chemistry. *Phys Chem Chem Phys* 8:2101–2116. doi:[10.1039/b600519p](https://doi.org/10.1039/b600519p)
 11. Zein El Abedin S, Saad AY, Farag HK, Borisenko N, Liu QX, Endres F (2007) Electrodeposition of selenium, indium and copper in an air- and water-stable ionic liquid at variable temperatures. *Electrochim Acta* 52:2746–2754. doi:[10.1016/j.electacta.2006.08.064](https://doi.org/10.1016/j.electacta.2006.08.064)
 12. Chen PY, Hussey CL (2007) The electrodeposition of Mn and Zn–Mn alloys from the room-temperature tri-*n*-butylmethylammonium bis((trifluoromethane)sulfonyl)imide ionic liquid. *Electrochim Acta* 52:1857–1864. doi:[10.1016/j.electacta.2006.07.049](https://doi.org/10.1016/j.electacta.2006.07.049)
 13. Abbott AP, Capper G, Davies DL, Rasheed RK, Tambyrajah V (2003) Novel solvent properties of choline chloride/urea mixtures. *Chem Commun* 1: 70–71. doi:[10.1039/b210714g](https://doi.org/10.1039/b210714g)
 14. Abbott AP, Boothby D, Capper G, Davies DL, Rasheed RK (2004) Deep eutectic solvents formed between choline chloride and carboxylic acids: versatile alternatives to ionic liquids. *J Am Chem Soc* 126:9142–9147. doi:[10.1021/ja048266j](https://doi.org/10.1021/ja048266j)
 15. Hamad AA, Hayyan M, AlSaadi MA, Hashim MA (2015) Potential applications of deep eutectic solvents in nanotechnology. *Chem Eng J* 273:551–567. doi:[10.1016/j.cej.2015.03.091](https://doi.org/10.1016/j.cej.2015.03.091)
 16. Carriazo D, Serrano MC, Gutiérrez MC, Ferrer ML, Monte F (2012) Deep-eutectic solvents playing multiple roles in the synthesis of polymers and related materials. *Chem Soc Rev* 41:4996–5014. doi:[10.1039/c2cs15353j](https://doi.org/10.1039/c2cs15353j)
 17. Deferm C, Hulsege J, Möller C, Thijs B (2013) Erratum to: electrochemical dissolution of metallic platinum in ionic liquids. *J Appl Electrochem* 43:797–804. doi:[10.1007/s10800-013-0555-0](https://doi.org/10.1007/s10800-013-0555-0)
 18. Dai YT, Spronsen JV, Witkamp GJ, Verpoorte R, Choi YH (2013) Natural deep eutectic solvents as new potential media for green technology. *Anal Chim Acta* 766:61–68. doi:[10.1016/j.aca.2012.12.019](https://doi.org/10.1016/j.aca.2012.12.019)
 19. Böck R, Lanzinger G, Freudenberger R, Mehner T, Nickel D, Scharf I, Lampke T (2013) Effect of additive and current mode on surface morphology of palladium films from a non-aqueous deep eutectic solution (DES). *J Appl Electrochem* 43:1207–1216. doi:[10.1007/s10800-013-0608-4](https://doi.org/10.1007/s10800-013-0608-4)
 20. Abbott AP, Ttaib KE, Frisch G, Ryder KS, Weston D (2012) The electrodeposition of silver composites using deep eutectic solvents. *Phys Chem Chem Phys* 14:2443–2449. doi:[10.1039/c2cp23712a](https://doi.org/10.1039/c2cp23712a)
 21. Abbott AP, Capper G, Davies DL, Rasheed RK, Shikotra P (2005) Selective extraction of metals from mixed oxide matrixes using choline-based ionic liquids. *Inorg Chem* 44:6497–6499. doi:[10.1021/ic0505450](https://doi.org/10.1021/ic0505450)
 22. Abbott AP, Capper G, Davies DL, McKenzie KJ, Obi SU (2006) Solubility of metal oxides in deep eutectic solvents based on choline chloride. *J Chem Eng Data* 51:1280–1282. doi:[10.1021/je060038c](https://doi.org/10.1021/je060038c)
 23. Abbott AP, Collins J, Dalrymple L, Harris RC, Mistry R, Qiu F, Scheirer J, Wise WR (2009) Processing of electric arc furnace dust using deep eutectic solvents. *Aust J Chem* 62:341–347. doi:[10.1071/CH08476](https://doi.org/10.1071/CH08476)
 24. Tsuda T, Boyd LE, Kuwabata S, Hussey CL (2010) Electrochemistry of copper(I) oxide in the 66.7–33.3 mol % urea–choline chloride room-temperature eutectic melt. *J Electrochem Soc* 157:F96–F103. doi:[10.1149/1.3377117](https://doi.org/10.1149/1.3377117)
 25. Yang HX, Reddy RG (2014) Electrochemical deposition of zinc from zinc oxide in 2:1 urea/choline chloride ionic liquid. *Electrochim Acta* 147:513–519. doi:[10.1016/j.electacta.2014.09.137](https://doi.org/10.1016/j.electacta.2014.09.137)
 26. Yang HX, Reddy RG (2014) Fundamental studies on electrochemical deposition of lead from lead oxide in 2:1 urea/choline chloride ionic liquids. *J Electrochem Soc* 161:D586–D592. doi:[10.1149/2.1161410jes](https://doi.org/10.1149/2.1161410jes)
 27. Zhang QB, Wang R, Chen KH, Hua YX (2014) Electrolysis of solid copper oxide to copper in Choline chloride–EG eutectic melt. *Electrochim Acta* 121:78–82. doi:[10.1016/j.electacta.2013.12.114](https://doi.org/10.1016/j.electacta.2013.12.114)
 28. Ru JJ, Hua YX, Wang D, Xu CY, Li J, Li Y, Zhou ZR, Gong K (2015) Mechanistic insight of in situ electrochemical reduction of solid PbO to lead in ChCl–EG deep eutectic solvent. *Electrochim Acta* 186:455–464. doi:[10.1016/j.electacta.2015.11.013](https://doi.org/10.1016/j.electacta.2015.11.013)
 29. Ru JJ, Hua YX, Wang D, Xu CY, Zhang QB, Li J, Li Y (2016) Dissolution-electrodeposition pathway and bulk porosity on the impact of in situ reduction of solid PbO in deep eutectic solvent. *Electrochim Acta* 196:56–66. doi:[10.1016/j.electacta.2016.02.181](https://doi.org/10.1016/j.electacta.2016.02.181)
 30. Xie XL, Zou XL, Lu XG, Lu CY, Cheng HW, Xu Q, Zhou ZF (2016) Electrodeposition of Zn and Cu–Zn alloy from ZnO/CuO precursors in deep eutectic solvent. *Appl Surf Sci* 385:481–489. doi:[10.1016/j.apsusc.2016.05.138](https://doi.org/10.1016/j.apsusc.2016.05.138)
 31. Xie XL, Zou XL, Lu XG, Zheng K, Cheng HW, Xu Q, Zhou ZF (2016) Voltammetric study and electrodeposition of Cu from CuO in deep eutectic solvents. *J Electrochem Soc* 163:D537–D543. doi:[10.1149/2.1241609jes](https://doi.org/10.1149/2.1241609jes)
 32. Prathish KP, Carvalho RC, Brett CMA (2014) Highly sensitive poly(3,4-ethylenedioxythiophene) modified electrodes by electropolymerisation in deep eutectic solvents. *Electrochem Commun* 44:8–11. doi:[10.1016/j.elecom.2014.03.026](https://doi.org/10.1016/j.elecom.2014.03.026)
 33. Chu QW, Liang J, Hao JC (2014) Electrodeposition of zinc-cobalt alloys from choline chloride–urea ionic liquid. *Electrochim Acta* 115:499–503. doi:[10.1016/j.electacta.2013.10.204](https://doi.org/10.1016/j.electacta.2013.10.204)
 34. Yang HY, Guo XW, Chen XB, Wang SH, Wu GH, Ding WJ, Birbilis N (2012) On the electrodeposition of nickel–zinc alloys from a eutectic-based ionic liquid. *Electrochim Acta* 63:131–138. doi:[10.1016/j.electacta.2011.12.070](https://doi.org/10.1016/j.electacta.2011.12.070)
 35. Li RQ, Chu QW, Liang J (2015) Electrodeposition and characterization of Ni–SiC composite coatings from deep eutectic solvent. *RSC Adv* 5:44933–44942. doi:[10.1039/c5ra05918f](https://doi.org/10.1039/c5ra05918f)
 36. Scharifker B, Hills G (1983) Theoretical and experimental studies of multiple nucleation. *Electrochim Acta* 28:879–889. doi:[10.1016/0013-4686\(83\)85163-9](https://doi.org/10.1016/0013-4686(83)85163-9)
 37. Abbott AP, Barron JC, Frisch G, Gurman S, Ryder KS, Silva AF (2011) Double layer effects on metal nucleation in deep eutectic solvents. *Phys Chem Chem Phys* 13:10224–10231. doi:[10.1039/c0cp02244f](https://doi.org/10.1039/c0cp02244f)
 38. Lin YP, Selman JR (1993) Electrodeposition of Ni–Zn alloy: II. Electrocrystallization of Zn, Ni, and Ni–Zn alloy. *J Electrochem Soc* 140:1304–1311. doi:[10.1149/1.2220975](https://doi.org/10.1149/1.2220975)
 39. Haerens K, Matthijs E, Binnemans K, Bruggen BV (2009) Electrochemical decomposition of choline chloride based ionic liquid analogues. *Green Chem* 11:1357–1365. doi:[10.1039/b906318h](https://doi.org/10.1039/b906318h)

40. Sun HJ, Yu LP, Jin XB, Hu XH, Wang DH, Chen GZ (2005) Unusual anodic behaviour of chloride ion in 1-butyl-3-methylimidazolium hexafluorophosphate. *Electrochem Commun* 7:685–691. doi:[10.1016/j.elecom.2005.04.020](https://doi.org/10.1016/j.elecom.2005.04.020)
41. Juškėnas R, Karpavičienė V, Pakštas V, Selskis A, Kapočius V (2007) Electrochemical and XRD studies of Cu–Zn coatings electrodeposited in solution with D-mannitol. *J Electroanal Chem* 602:237–244. doi:[10.1016/j.jelechem.2007.01.004](https://doi.org/10.1016/j.jelechem.2007.01.004)
42. Langford JI, Wilson AJC (1978) Scherrer after sixty years: a survey and some new results in the determination of crystallite size. *J Appl Cryst* 11:102–113. doi:[10.1107/S0021889878012844](https://doi.org/10.1107/S0021889878012844)
43. Beattie SD, Dahn JR (2003) Comparison of electrodeposited copper-zinc alloys prepared individually and combinatorially. *J Electrochem Soc* 150:C802–C806. doi:[10.1149/1.1615998](https://doi.org/10.1149/1.1615998)
44. Chaaya AA, Viter R, Bechelany M, Alute Z, Erts D, Zalesskaya A, Kovalevskis K, Rouessac V, Smytyna V, Miele P (2013) Evolution of microstructure and related optical properties of ZnO grown by atomic layer deposition. *Beilstein J Nanotechnol* 4:690–698. doi:[10.3762/bjnano.4.78](https://doi.org/10.3762/bjnano.4.78)
45. Guo L, Searson PC (2010) On the influence of the nucleation overpotential on island growth in electrodeposition. *Electrochim Acta* 55:4086–4091. doi:[10.1016/j.electacta.2010.02.038](https://doi.org/10.1016/j.electacta.2010.02.038)
46. Vreese PD, Skoczylas A, Matthijs E, Fransaeer J, Binnemans K (2013) Electrodeposition of copper–zinc alloys from an ionic liquid-like choline acetate electrolyte. *Electrochim Acta* 108:788–794. doi:[10.1016/j.electacta.2013.06.140](https://doi.org/10.1016/j.electacta.2013.06.140)
47. Karahan IH, Özdemir R (2014) Effect of Cu concentration on the formation of $\text{Cu}_{1-x}\text{Zn}_x$ shape memory alloy thin films. *Appl Surf Sci* 318:100–104. doi:[10.1016/j.apsusc.2014.01.119](https://doi.org/10.1016/j.apsusc.2014.01.119)
48. Zhang JL, Gu CD, Fashu S, Tong YY, Huang ML, Wang XL, Tu JP (2015) Enhanced corrosion resistance of Co–Sn alloy coating with a self-organized layered structure electrodeposited from deep eutectic solvent. *J Electrochem Soc* 162:D1–D8. doi:[10.1149/2.0231501jes](https://doi.org/10.1149/2.0231501jes)
49. Wang SG, Shen CB, Long K, Yang HY, Wang FH, Zhang ZD (2005) Preparation and electrochemical corrosion behavior of bulk nanocrystalline ingot iron in HCl acid solution. *J Phys Chem B* 109:2499–2503. doi:[10.1021/jp046297v](https://doi.org/10.1021/jp046297v)
50. Mountassir Z, Srhiri A (2007) Electrochemical behaviour of Cu–40Zn in 3% NaCl solution polluted by sulphides: effect of aminotriazole. *Corros Sci* 49:1350–1361. doi:[10.1016/j.corsci.2006.07.001](https://doi.org/10.1016/j.corsci.2006.07.001)
51. Chang LM, Chen D, Liu JH, Zhang RJ (2009) Effects of different plating modes on microstructure and corrosion resistance of Zn–Ni alloy coatings. *J Alloys Compd* 479:489–493. doi:[10.1016/j.jallcom.2008.12.108](https://doi.org/10.1016/j.jallcom.2008.12.108)